

# Variability in Quasar Broad Absorption Line Outflows I. Trends in the Short-Term versus Long-Term Data

D. M. Capellupo<sup>1</sup> \*, F. Hamann<sup>1</sup>, J. C. Shields<sup>2</sup>, P. Rodríguez Hidalgo<sup>3</sup>, and T.A. Barlow<sup>4</sup>

<sup>1</sup>*Department of Astronomy, University of Florida, Gainesville, FL 32611*

<sup>2</sup>*Department of Physics & Astronomy, Ohio University, Athens, OH 45701*

<sup>3</sup>*Department of Astronomy and Astrophysics, Pennsylvania State University, University Park, PA 16802*

<sup>4</sup>*Infrared Processing and Analysis Center, California Institute of Technology, Pasadena, CA 91125*

29 May 2018

## ABSTRACT

Broad absorption lines (BALs) in quasar spectra identify high velocity outflows that likely exist in all quasars and could play a major role in feedback to galaxy evolution. The variability of BALs can help us understand the structure, evolution, and basic physical properties of the outflows. Here we report on our first results from an ongoing BAL monitoring campaign of a sample of 24 luminous quasars at redshifts  $1.2 < z < 2.9$ , focusing on CIV  $\lambda 1549$  BAL variability in two different time intervals: 4 to 9 months (short-term) and 3.8 to 7.7 years (long-term) in the quasar rest-frame. We find that 39% (7/18) of the quasars varied in the short-term, whereas 65% (15/23) varied in the long-term, with a larger typical change in strength in the long-term data. The variability occurs typically in only portions of the BAL troughs. The components at higher outflow velocities are more likely to vary than those at lower velocities, and weaker BALs are more likely to vary than stronger BALs. The fractional change in BAL strength correlates inversely with the strength of the BAL feature, but does not correlate with the outflow velocity. Both the short-term and long-term data indicate the same trends. The observed behavior is most readily understood as a result of the movement of clouds across the continuum source. If the crossing speeds do not exceed the local Keplerian velocity, then the observed short-term variations imply that the absorbers are  $< 6$  pc from the central quasar.

**Key words:** galaxies: active – quasars:general – quasars:absorption lines.

## 1 INTRODUCTION

Accretion disk outflows play a key role in the physics of quasars and their environs. Quasar outflows may be an integral part of the accretion process and the growth of supermassive black holes (SMBHs), by allowing the accreting material to release angular momentum. These outflows may also provide enough kinetic energy feedback to have an effect on star formation in the quasar host galaxies, to aid in ‘unveiling’ dust-enshrouded quasars, and to help distribute metal-rich gas to the intergalactic medium (e.g., Di Matteo, Springel, & Hernquist 2005, Moll et al. 2007).

The location and three-dimensional structure of quasar outflows are poorly understood. Sophisticated models have been developed that envision these outflows as arising from a rotating accretion disk, with acceleration to high speeds by radiative and/or magneto-centrifugal forces (Murray et al.

1995, Proga & Kallman 2004, Proga 2007, Everett 2005). Improved observational constraints are needed to test these models and allow estimation of mass loss rates, kinetic energy yields, and the role of quasar outflows in feedback to the surrounding environment. In this paper, we focus on the most prominent signatures of accretion disk outflows that appear in quasar spectra, the broad absorption lines (BALs). BALs are defined to have velocity widths  $> 2000$  km s<sup>-1</sup> at absorption depths  $> 10\%$  below the continuum (Weymann et al. 1991), and they appear in the spectra of  $\sim 10\text{--}15\%$  of quasars (Reichard et al. 2003a, Trump et al. 2006). Since only a fraction of quasar spectra display these features, the presence of BALs could represent a phase in the evolution of a quasar and/or particular orientations where the outflow lies between us and the quasar emission sources. Other studies have found support for the latter scenario, given the similarity of various properties between BALQSOs and non-BALQSOs (e.g., Weymann et al. 1991, Shen et al. 2008).

\* E-mail: dancaps@astro.ufl.edu (DMC)

Studying the variability in these absorption features can provide important insight into the structure and dynamics of the outflows. For example, we can use information about short-term variability to place constraints on the distance of the absorbing material from the central SMBH. The more quickly the absorption is varying, the closer the absorber is to the central source, based on nominally shorter crossing times for moving clouds (Hamann et al. 2008 and §5 below) or the higher densities required for shorter recombination times (Hamann et al. 1997). Long-term variability measurements provide information on the homogeneity and stability of the outflow. A lack of variability on long time-scales implies a smooth flow with a persistent structure. General variability results provide details on the size, kinematics, and internal makeup of sub-structures within the flows. Variability studies can also address the evolution of these outflows as the absorption lines are seen to come and go, or one type of outflow feature evolves into another (e.g., Hamann et al. 2008).

A small number of previous studies have investigated variability in BALs, emphasizing C IV  $\lambda 1549$  because of its prominence and ease of measurement. Barlow (1993) carried out a study of 23 BALQSOs, covering time-scales of  $\Delta t \lesssim 1 \text{ yr}^1$ . Lundgren et al. (2007) used Sloan Digital Sky Survey (SDSS) spectra of 29 quasars to study C IV BAL variability on similar time-scales. Gibson et al. (2008) studied variability on longer time-scales (3-6 years) by combining data for 13 BALQSOs from the Large Bright Quasar Survey (LBQS) and SDSS. Gibson et al. (2010) reports on variability on multi-month to multi-year time-scales, using 3-4 epochs of data for 9 BALQSOs. They also compare variability in Si IV absorption to variability in C IV absorption in their sample.

In the present study, we go beyond existing work by carrying out a monitoring program of BALQSOs from the sample of Barlow (1993). This strategy provides BAL variability data covering longer time-scales as well as a wider range in time-scales within individual sources. We include archival spectra from the SDSS, when available, to augment the temporal sampling. This paper reports our results for C IV  $\lambda 1549$  variability with measurements selected to enable comparison between short-term (0.35 to 0.75 yr) and long-term (3.8 to 7.7 yr) behavior. We identify trends in the data with velocity and the depth of the absorption. We avoid using equivalent width (EW) measurements, which can minimize a change that occurs in a portion of a much wider trough. In subsequent papers, we will discuss variability properties in the entire data set, including more epochs on individual quasars, sampling in a much shorter time domain, and comparisons between the C IV and Si IV  $\lambda 1400$  variabilities to place constraints on the outflow ionizations and column densities. Section 2 below discusses the observations and the quasar sample. Section 3 describes the steps we followed to identify the C IV BALs and where they varied. Section 4 describes our results, and Section 5 discusses the implications of these results with comparisons to previous work.

## 2 DATA AND QUASAR SAMPLE

Between 1988 and 1992, Barlow (1993) and his collaborators (e.g., Barlow et al. 1992) obtained spectra for 28 BALQSOs with the Lick Observatory 3-m Shane Telescope. They obtained multi-epoch spectra for 23 of these quasars for a study of short-term BAL variability. They selected these objects from already known BALQSOs, with redshifts of 1.2 to 2.9. When selecting objects for their monitoring program, they gave preference to quasars known to have either absorption line or photometric variability. However, in most cases, this information was not available, and they selected more quasars at higher redshifts due to higher detector sensitivity at longer wavelengths. While this sample of BALQSOs is not randomly selected, it does cover a wide range of BAL strengths (see Table 1 and Figure 1).

Barlow (1993) used the Lick Observatory Kast spectrograph to obtain spectra with settings for high resolution,  $R \equiv \lambda/\Delta\lambda \approx 1300$  ( $230 \text{ km s}^{-1}$ ), and moderate resolution,  $R \approx 600$  ( $530 \text{ km s}^{-1}$ ). Most of the objects were observed at both settings. For our analysis of these data discussed below, we used the high-resolution observations for most sources. In some cases, only a moderate-resolution observation is available or choosing the high-resolution observation would compromise wavelength coverage. Since BALs have a width of at least  $2000 \text{ km s}^{-1}$ , a resolution of  $530 \text{ km s}^{-1}$  is sufficient to detect changes in their profiles.

Starting in January 2007, we have been using the MDM Observatory 2.4-m Hiltner telescope to reobserve the BALQSOs in the sample of Barlow (1993), with the goal of monitoring BAL variability over a wide range of time-scales, from <1 month to nearly 8 years. We also supplemented our data set with spectra from the Sloan Digital Sky Survey (SDSS). So far, we have over 120 spectra for 24 BALQSOs, and we continue to collect more data. We note that two of these objects are not strictly BALQSOs because they have a balnicity index of zero (see §3.2 below). Nonetheless, we include them in our sample because they do have broad absorption features at velocities that we include in our variability analysis (§3.3).

We used the MDM CCDS spectrograph with a 350 groove per mm grating in first order and a  $1''$  slit to yield a spectral resolution of  $R \approx 1200$  ( $250 \text{ km s}^{-1}$ ), with wavelength coverage of  $\sim 1600 \text{ \AA}$ . The spectrograph was rotated between exposures to maintain approximate alignment of the slit with the parallactic angle, to minimize wavelength-dependent slit losses. The wavelength range for each observation was determined based on the redshift of the target quasar such that the coverage was blue enough to include the Ly $\alpha$  emission and red enough to include the C IV emission feature. The coadded exposure times were typically 1-2 hours per source.

We reduced the data using standard reduction techniques with the IRAF<sup>2</sup> software. The data are flux calibrated on a relative scale to provide accurate spectral shapes. Ab-

<sup>1</sup> Throughout this paper, all time intervals are measured in years in the rest frame of the quasar.

<sup>2</sup> The Image Reduction and Analysis Facility (IRAF) is distributed by the National Optical Astronomy Observatories (NOAO), which is operated by the Association of Universities for Research in Astronomy (AURA), Inc., under cooperative agreement with the National Science Foundation.

solite flux calibrations were generally not obtained due to weather or time constraints.

The Sloan Digital Sky Survey is an imaging and spectroscopic survey of the sky at optical wavelengths. The data were acquired by a dedicated 2.5-m telescope at Apache Point Observatory in New Mexico. The spectra cover the observer-frame optical and near-infrared, from 3800 to 9200 Å, and the resolution is  $R \approx 2000$  ( $150 \text{ km s}^{-1}$ ). For spectra, typically three exposures were taken for 15 minutes each, and more exposures were taken in poor conditions to achieve a target signal-to-noise ratio. The multiple observations were then co-added (Adelman-McCarthy et al. 2008). The SDSS includes observations of 11 of the quasars in the Lick sample. However, 3 of the SDSS observations are unusable because the redshifts of those quasars are too low for the C IV BALs to appear in the SDSS spectra. Therefore, we have usable SDSS spectra for 8 of the objects in our sample, and they were taken between 2000 and 2006.

### 3 ANALYSIS

#### 3.1 Short-Term and Long-Term Data Sets

From the data in our BAL monitoring campaign, for each object, we select one pair of observations for the short-term analysis and one pair for the long-term analysis. For the long-term analysis, we want the longest time baseline possible. The first observation for each object is the earliest Lick observation with the highest available resolution as well as wavelength coverage that extends from the Ly $\alpha$  emission line through the C IV emission line. For the second observation for each object, we use the most recent MDM spectrum. We have long-term data for 23 objects, with resulting  $\Delta t$  of 3.8 to 7.7 years. We note that for certain objects, the redshift is low enough that the Ly $\alpha$  emission line is not shifted into the wavelength coverage of our data and therefore is not present in some of the spectra (e.g., 0946+3009).

For the short-term analysis, the range in the values of  $\Delta t$  among the objects should be small, while including as many objects as possible. The best compromise we found was a range for  $\Delta t$  of 0.35 to 0.75 yr, which allows us to include 18 objects in the short-term analysis. In order to include this many objects, we use data for some objects that only covers the region from the Si IV emission to the C IV emission, which is sufficient for the analysis in this paper. These observations were selected separately from the long-term epochs and were chosen to fit into this  $\Delta t$  interval. These observations were taken before or at any time in between the two long-term observations. There is one object for which we have short-term Lick data, but no long-term data (2225-0534), so we have in total 24 objects in our full sample.

#### 3.2 Characterizing the Quasar Sample

Table 1 summarizes our full sample of long-term and short-term data, as described above. The first four columns provide information on all 24 quasars.  $z_{em}$  is the emission red-

shift<sup>3</sup>, and BI is the “balnicity index,” as described below. The remaining columns are separated into the short-term analysis and long-term analysis. The columns with “vary?” have either Yes or No values to indicate variability anywhere in the C IV troughs (refer to §4), and  $\Delta t$  is the time difference (in years) in the quasar frame between observations. The observations from 1988 to 1992 are from Lick, the observations from 2000 to 2006 are from SDSS, and the observations from 2007 to 2008 are from MDM.

Figure 1 contains spectra for all 24 objects, showing the long-term comparisons between a Lick spectrum and an MDM spectrum. The one exception is 2225-0534, for which we only have short-term Lick data. The velocity scale is based on the wavelength of C IV in the observed frame calculated from the redshifts given in Table 1. We use a weighted average of the C IV doublet wavelengths, i.e., 1549.05 Å.

The balnicity index (BI, Weymann et al. 1991) is designed to differentiate between BALQSOs and non-BALQSOs and provide a measure of the BAL strength, expressed as an equivalent width in units of velocity. It quantifies absorption that is blueshifted between  $-3000$  and  $-25000 \text{ km s}^{-1}$  from the C IV emission line centre, is at least  $\sim 10\%$  below the continuum, and is wider than  $2000 \text{ km s}^{-1}$ . By this definition, if a quasar has a BI greater than zero, then it is classified as a BALQSO. The highest possible value of BI is 20,000.

We measure BI in one observation per object to characterize the sample and allow for comparison with BALQSOs in other studies. We do not use BI in our variability analysis. In order to normalize the spectra and measure BI, and later absorption strength (see §3.3), we first had to fit a pseudo-continuum to one spectrum per quasar, which includes the quasar’s continuum emission plus the broad emission lines. We adopt the Lick observations used in the long-term analysis as our fiducial epoch for which we fit the pseudo-continuum and measure BI. We constructed this pseudo-continuum by fitting a power-law to the continuum away from any emission or absorption lines, and then adding to that an estimate of the C IV and, if necessary, the Si IV broad emission line (BEL) profiles<sup>4</sup>. To fit the continuum, we fit a power-law function to two regions on the spectrum that are free of strong emission lines. The preferred wavelength ranges for the fits were 1270 to 1350 Å and 1680 to 1800 Å. These ranges were adjusted to avoid emission and absorption features as much as possible or due to the limits of the wavelength coverage. Fitting the C IV emission is complicated by, for example, potential asymmetries in the emission profiles and absorption in the emission region (e.g., Reichard et al. 2003b). Therefore, we are flexible in our fitting routine, using between 1 and 3 gaussians to define the line profile. The gaussians have no physical meaning, and we simply use them for obtaining a reasonable fit to the profile. If there is any absorption on top of the emission, we ignore those wavelengths when defining the fit. In cases where the absorption is wide enough that it obscures up to half of the emission

<sup>3</sup> The values of  $z_{em}$  were obtained from the NASA/IPAC Extragalactic Database (NED), which is operated by the Jet Propulsion Laboratory, California Institute of Technology, under contract with the National Aeronautics and Space Administration.

<sup>4</sup> Note that the feature we attribute to Si IV may also include O IV]  $\lambda 1400$  emission.

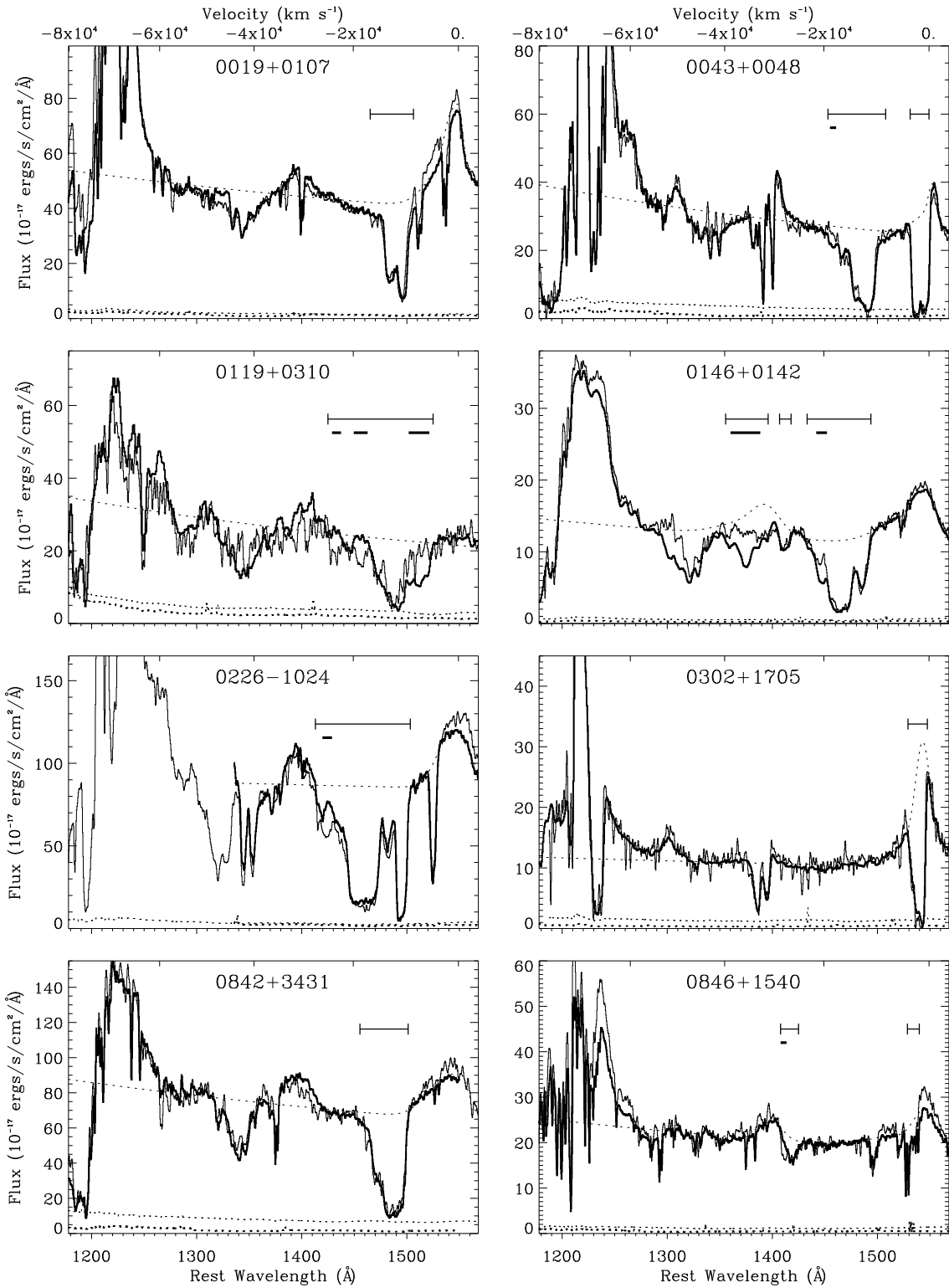


**Figure 1.** Smoothed spectra of all 24 quasars in our sample, showing the long-term comparisons between a Lick Observatory spectrum (bold curves) and the most recent MDM data (thin curves). The one exception is 2225-0534, for which we only have short-term data (see Table 1). The vertical flux scale applies to the Lick data, and the MDM spectrum has been scaled to match the Lick data in the continuum. The dashed curves show our pseudo-continuum fits. The thin horizontal bars indicate intervals of BAL absorption included in this study, and the thick horizontal bars indicate intervals of variation within the BALs. The formal  $1\sigma$  errors are shown near the bottom of each panel.

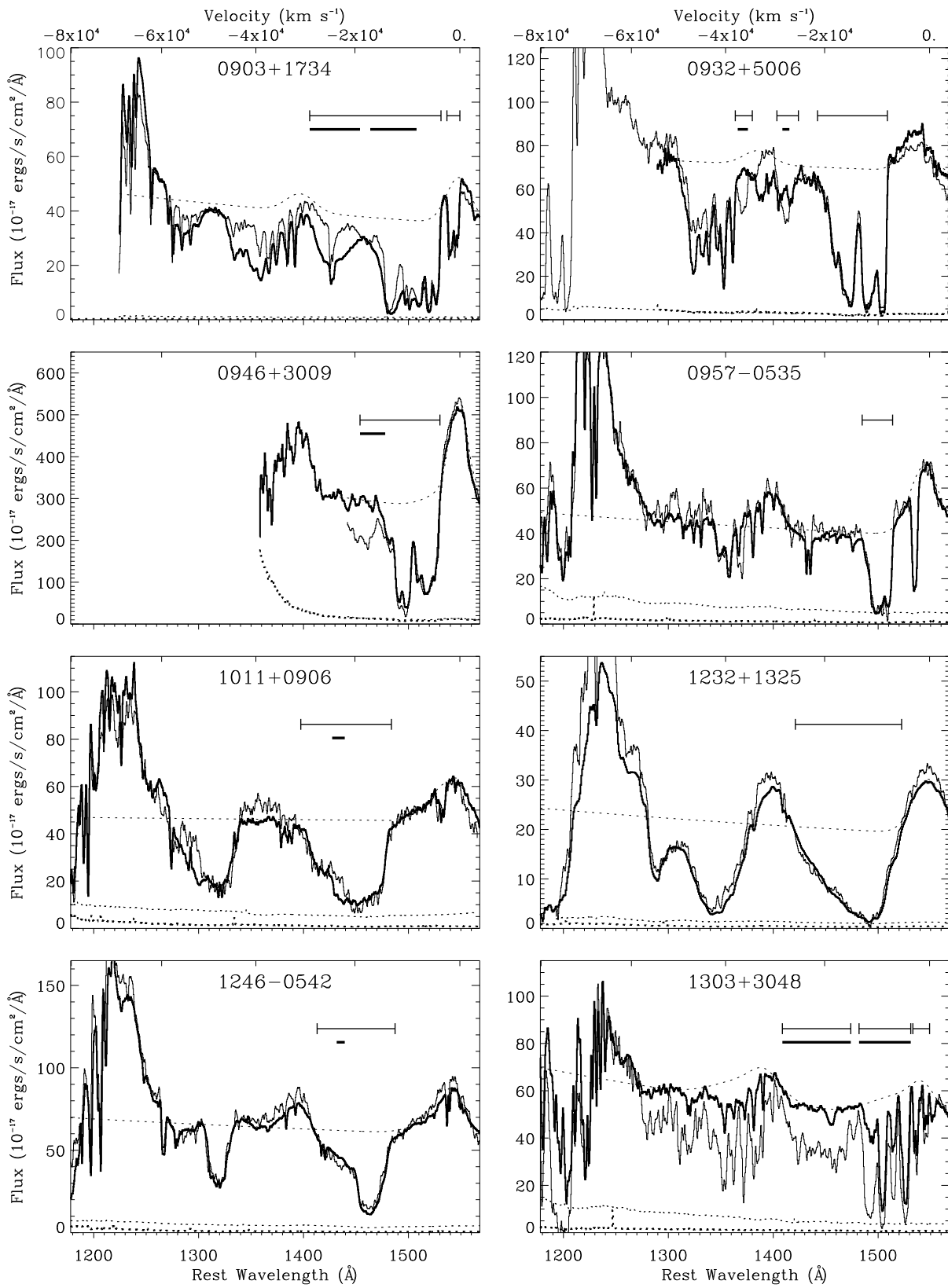


Figure 1. continued...

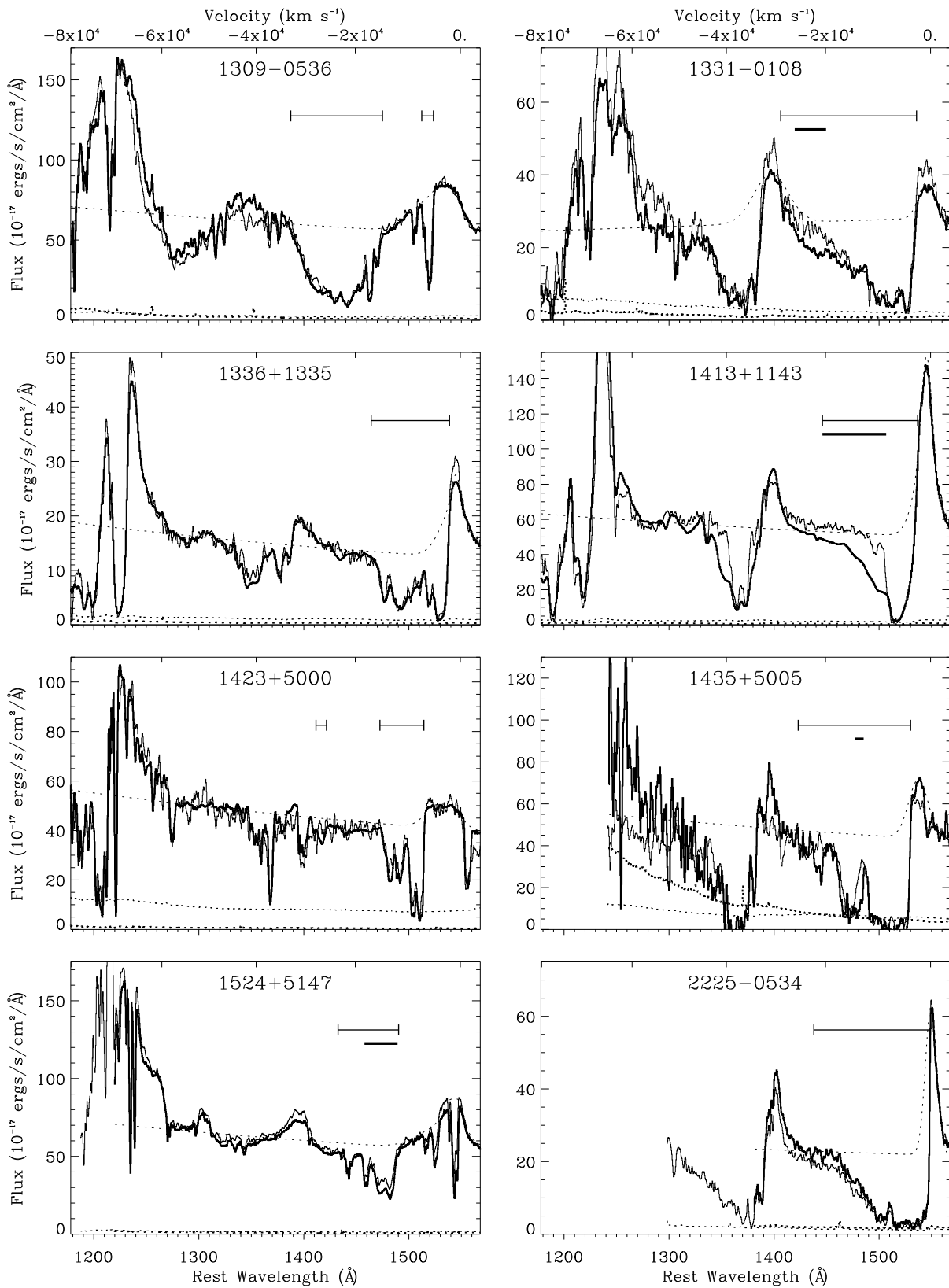


Figure 1. continued...

**Table 1.** Quasar Data and CIV Variability Results

| Coord.<br>(1950.0) | Name            | $z_{em}$ | BI    | Short-Term           |         |            |       | Long-Term            |         |            |       |
|--------------------|-----------------|----------|-------|----------------------|---------|------------|-------|----------------------|---------|------------|-------|
|                    |                 |          |       | Obs. 1               | Obs. 2  | $\Delta t$ | Vary? | Obs. 1               | Obs. 2  | $\Delta t$ | Vary? |
| 0019+0107          | UM 232          | 2.13     | 2290  | 1989.84              | 1991.86 | 0.65       | N     | 1989.84              | 2007.04 | 5.50       | N     |
| 0043+0048          | UM 275          | 2.14     | 4330  | 2000.69              | 2001.79 | 0.35       | N     | 1991.86              | 2008.03 | 5.15       | Y     |
| 0119+0310          | AD85 D08        | 2.09     | 5170  | 1989.85 <sup>a</sup> | 1991.86 | 0.65       | Y     | 1989.85 <sup>a</sup> | 2007.07 | 5.57       | Y     |
| 0146+0142          | UM 141          | 2.91     | 5780  | 1988.93 <sup>a</sup> | 1991.86 | 0.75       | Y     | 1988.93 <sup>a</sup> | 2007.05 | 4.64       | Y     |
| 0226-1024          | WFM91 0226-1024 | 2.25     | 7770  |                      |         |            |       | 1991.87              | 2007.04 | 4.66       | Y     |
| 0302+1705          | HB89 0302+170   | 2.89     | 0     |                      |         |            |       | 1989.84 <sup>a</sup> | 2007.05 | 4.42       | N     |
| 0842+3431          | CSO 203         | 2.15     | 4430  | 2007.04              | 2008.35 | 0.42       | Y     | 1990.90              | 2008.35 | 5.54       | N     |
| 0846+1540          | H 0846+1540     | 2.93     | 0     | 1990.16              | 1992.19 | 0.52       | Y     | 1992.19              | 2007.05 | 3.78       | Y     |
| 0903+1734          | HB89 0903+175   | 2.77     | 10700 | 2006.31              | 2008.28 | 0.52       | Y     | 1989.26 <sup>a</sup> | 2008.28 | 5.04       | Y     |
| 0932+5006          | SBS 0932+501    | 1.93     | 7920  | 1989.84              | 1991.10 | 0.43       | N     | 1989.84              | 2008.28 | 6.30       | Y     |
| 0946+3009          | PG 0946+301     | 1.22     | 5550  | 1991.10              | 1992.23 | 0.51       | Y     | 1991.10              | 2008.28 | 7.74       | Y     |
| 0957-0535          | HB89 0957-055   | 1.81     | 2670  | 1990.89              | 1992.32 | 0.51       | N     | 1992.32              | 2008.35 | 5.70       | N     |
| 1011+0906          | HB89 1011+091   | 2.27     | 6100  | 2007.07              | 2008.35 | 0.39       | N     | 1992.19              | 2008.35 | 4.94       | Y     |
| 1232+1325          | HB89 1232+134   | 2.36     | 11000 |                      |         |            |       | 1989.26 <sup>a</sup> | 2008.03 | 5.58       | N     |
| 1246-0542          | HB89 1246-057   | 2.24     | 4810  | 2007.04              | 2008.35 | 0.40       | N     | 1992.19              | 2008.35 | 4.99       | Y     |
| 1303+3048          | HB89 1303+308   | 1.77     | 1390  | 2007.04              | 2008.28 | 0.45       | N     | 1992.32              | 2008.28 | 5.76       | Y     |
| 1309-0536          | HB89 1309-056   | 2.22     | 4690  |                      |         |            |       | 1992.19              | 2007.04 | 4.61       | N     |
| 1331-0108          | UM 587          | 1.88     | 10400 | 2007.04              | 2008.28 | 0.43       | N     | 1992.32              | 2008.28 | 5.55       | Y     |
| 1336+1335          | HB89 1336+135   | 2.45     | 7120  |                      |         |            |       | 1989.26 <sup>a</sup> | 2008.28 | 5.52       | N     |
| 1413+1143          | HB89 1413+117   | 2.56     | 6810  | 2006.31              | 2008.28 | 0.55       | Y     | 1989.26 <sup>a</sup> | 2008.28 | 5.35       | Y     |
| 1423+5000          | CSO 646         | 2.25     | 3060  | 2007.07              | 2008.35 | 0.39       | N     | 1992.32              | 2008.35 | 4.93       | N     |
| 1435+5005          | CSO 673         | 1.59     | 11500 |                      |         |            |       | 1992.19              | 2008.35 | 6.25       | Y     |
| 1524+5147          | CSO 755         | 2.88     | 2490  | 1989.60              | 1991.52 | 0.49       | N     | 1991.52              | 2008.28 | 4.32       | Y     |
| 2225-0534          | HB89 2225-055   | 1.98     | 7920  | 1988.46              | 1989.84 | 0.46       | N     |                      |         |            |       |

<sup>a</sup> These Lick observations were taken at the lower resolution setting ( $R \approx 600$ ; see §2).

line (e.g. 1413+1143), we assume the emission line is symmetric. In cases where the gaussian, or multiple-gaussian, fit did not provide the right shape and we have enough information about the profile (e.g. 1423+5000), we manually adjusted the fit to better match the C IV emission line.

For quasars where the C IV absorption is at a velocity that overlaps the Si IV emission, we also fit the Si IV emission line. If most, or all, of the Si IV emission feature is absorbed, we synthesized a Si IV profile by taking the C IV fit, shifting its centre wavelength to the location of Si IV, adjusting the FWHM (given the wider separation between the Si IV doublet lines), and scaling the emission strength by a factor of 0.342. This scale factor is based on composite quasar spectra from which Vanden Berk et al. (2001) found the typical strength of various emission lines. We relied on this scale factor in cases such as 0146+0142, where we have little information about the Si IV emission line. Otherwise, in a case such as 0846+1540, we fit between 1 and 3 gaussians to the Si IV line, as we did for the C IV emission, because we have more information about the profile of the Si IV emission line. The pseudo-continuum fits for each object are shown by the smooth dotted curves in Figure 1.

### 3.3 Measuring the BAL Variability

For each quasar, we compare the two spectra in our short-term and long-term intervals (see Table 1) to search for variability in the C IV BALs. First, we determined the velocity ranges over which BAL absorption occurs. These ranges might differ between the two observing epochs. We therefore

set the range to the extremes observed in either epoch. Our definition of these ranges is guided by the definition of BI, i.e. they must present contiguous absorption reaching  $\geq 10\%$  below the continuum across  $\geq 2000 \text{ km s}^{-1}$ . We do not follow the requirement that the absorption be blueshifted between  $-3000$  and  $-25000 \text{ km s}^{-1}$  because we want to include all C IV broad absorption in our analysis (as a result, our sample contains two objects, 0302+1705 and 0846+1540, with a BI of 0). In general, the C IV BALs occur between the Si IV and C IV emission lines, but some of the C IV absorption is blue-shifted enough that it appears blueward of the Si IV emission line center (e.g., 0146+0142). In these cases, we can confirm that the absorption blueward of the Si IV emission line is due to C IV, and not Si IV, because any significant Si IV absorption should be accompanied by C IV absorption at the same velocity. This is evident from numerous observations of BALQSOs where the Si IV and C IV absorption are clearly identified (e.g., Figure 1, Korista et al. 1993), and from theoretical considerations of the relative strengths of these lines (Hamann et al. 2008). Our sample includes broad absorption troughs from 0 to  $-40000 \text{ km s}^{-1}$ .

In order to compare any two spectra for variability in the defined absorption ranges, we scaled the spectra so that regions free of absorption and emission in each spectrum match. This is necessary because of uncertainties in the flux calibration and possible real changes in the quasar emissions. We applied a simple vertical scaling so that the spectra from each epoch match the fiducial Lick spectrum along the continuum redward of the C IV emission feature (i.e., from 1560 Å to the limit of the wavelength coverage), between the Si IV

and C IV emission ( $\sim 1425\text{-}1515 \text{ \AA}$ ), and between the Ly $\alpha$  and the Si IV emission ( $\sim 1305\text{-}1315 \text{ \AA}$ ). In nearly all cases, a simple scaling produced a good match between the spectra from different epochs. The results for the two long-term epochs are shown in Figure 1. In some cases, however, there were disparities in the overall spectral shape of the two spectra. To remove these disparities, we fit either a linear function (for 0903+1734, 1413+1143, and 1423+5000) or quadratic function (for 0019+0107 and 1309-0536) to the spectral regions that avoid the BALs in a ratio of the two spectra. We then multiplied this function by the comparison spectrum.

We identify BAL variability in velocity intervals that correspond to at least 2 resolution elements in the lower resolution Lick spectra, i.e.,  $1200 \text{ km s}^{-1}$ . Our procedure to identify variability intervals relies mainly on visual inspection because photon statistics alone are not sufficient for defining real variability. Most of the occurrences of variability recorded for this study are obvious by simple inspection. However, we also examined all cases of weak or possible variability to ensure that no occurrences of significant real variability are missed. We determined the significance of variability based on two criteria. First, we calculate the average flux and associated error within each variability interval and use that to place an error on the flux differences between the two spectra. We include in this study only the intervals of variability where the flux differences are at least 4-sigma. We emphasize that all of the intervals which varied by 4-sigma or more are readily identified by our initial inspection technique. Therefore, there is no danger of variable intervals being missed. However, the 4-sigma threshold alone can include spurious or highly uncertain variability results because of uncertainties not captured by the photon statistics. These additional uncertainties can arise from the flux calibration, a poorly constrained continuum placement, underlying emission line variability or our reconstruction of a severely absorbed emission line profile. We therefore apply a second significance criterion based on our assessment of these additional uncertainties. We take a conservative approach by excluding variability intervals where the additional uncertainties might be large (even if the flux difference passes the formal 4-sigma threshold described above). This second criterion caused the exclusion of just a few intervals. See below for examples. The velocity intervals finally classified as variable in the long-term data are indicated by bold horizontal lines in Figure 1.

To help clarify our assessments of the additional uncertainties, we point out some specific velocity intervals that pass the 4-sigma threshold and appear variable by casual inspection, but are nonetheless excluded from our analysis because the additional uncertainties are significant. For example, in 1246-0542, we do not include the region around  $-17,000 \text{ km s}^{-1}$  because the noise level in that portion of the trough makes it a very tenuous candidate for inclusion in the study. The region around  $-21,000 \text{ km s}^{-1}$  in 1435+5005 is a similar case because here the increased noise level of the spectra towards greater outflow velocities makes a determination of variability more uncertain. We note that the increased scatter in the data for these two objects is less noticeable in the smoothed spectra plotted in Figure 1. In a couple cases, a slight difference in the slope between two comparison spectra adds some uncertainty. In 1413+1143, the blue wing of the C IV trough in the MDM spectrum ex-

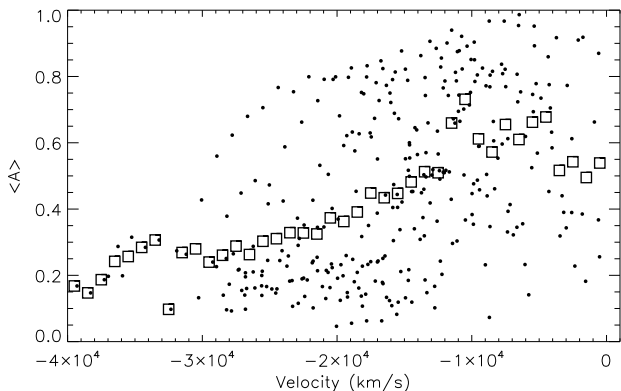


**Figure 2.** The average normalized absorption strength ( $\langle A \rangle$ ), calculated throughout all of the BALs in the quasars in our long-term subsample, as a function of the outflow velocity of the absorbing material. The individual points in each bin (with width  $1000 \text{ km s}^{-1}$ ) represent the  $\langle A \rangle$  for a single quasar, and the open squares represent the average of all points in that bin.

tends slightly above the defined continuum. This may be due to some anomaly in the flux calibration, so we define the blue end of the BAL (and the variability interval) as  $-20,600 \text{ km s}^{-1}$ . In 2225-0534, there is very little continuum available for matching the two comparison spectra, and this added uncertainty makes the small flux difference at the bluest portion of the BAL trough too tenuous to be included. A slight difference in slope between the two epochs could be responsible for any apparent changes in the wing of this BAL, and we do not have enough visible continuum to discount this possibility.

Identifying variability in the spectral regions which overlap the C IV and Si IV emission lines is further complicated by possible variability in the emission lines themselves (e.g., Wilhite et al. 2005). We record BAL variability in these spectral regions only if it is large compared to any reasonable change in the broad emission lines and/or the absorption changes abruptly over just portions of a BEL profile. For example, in 0146+0142, the interval from  $-38,800$  to  $-32,700 \text{ km s}^{-1}$  clearly shows BAL absorption weakening to approximately continuum level. In another case, 0932+5006, we include the intervals from  $-37,500$  to  $-35,400 \text{ km s}^{-1}$  and  $-28,400$  to  $-27,000 \text{ km s}^{-1}$  because there is clearly BAL absorption there in the MDM spectrum. We did not attribute the change in flux from approximately  $-34,000$  to  $-30,000 \text{ km s}^{-1}$  to a BAL because it is unclear what is the primary cause of variability in this interval. While the identifications of BAL absorption and variability in the regions overlapping C IV and Si IV emission are secure, the measurements of absorption strength ( $\langle A \rangle$ ; see below) in this region have added uncertainty since fitting the emission lines is more uncertain than fitting the continuum. When looking at correlations with velocity in this study, we identify trends using all the data, but also confirm the existence of these trends in the velocity range  $-27,000$  to  $-8,000 \text{ km s}^{-1}$ , which avoids the emission lines. For correlations with absorption strength (see below), since there are few cases of variability at the extremes of the examined velocity range, their inclusion does not significantly alter the plots or the final results.

In order to look for trends in the data, we calculated the

absorption strength as a function of velocity in each spectrum. We first normalized each spectrum using the pseudo-continuum fit (see §3.2) for that quasar. We can apply the pseudo-continua derived in §3.2 to the other epochs for each quasar because those epochs have already been scaled to match the fiducial Lick spectrum. However, we adjust the emission line fits in cases where the emission line varied. We define absorption strength,  $A$ , as the fraction of the normalized continuum flux removed by absorption ( $0 \leq A \leq 1$ ) within a specified velocity interval. A single  $A$  value is adopted for each velocity interval based on the average flux within that interval. If there is variability, then the absorption strength changed and we calculate the average absorption strength,  $\langle A \rangle$ , and the change in absorption strength,  $\Delta A$ , between the two epochs being compared. The velocity intervals used to calculate  $\langle A \rangle$  and  $\Delta A$  are defined to i) include only portions of the spectrum with BAL absorption and ii) clearly separate the spectral regions within BAL troughs that did and did not vary. Specifically, the variable and non-variable absorption regions are each divided into equal-sized bins, with a bin width of 1000 to 2000  $\text{km s}^{-1}$  depending on the velocity width of the region. This strategy makes the bin widths used to measure  $\langle A \rangle$  and  $\Delta A$  similar to the nominal width of 1200  $\text{km s}^{-1}$  used above, while providing the flexibility needed to begin and end at the boundaries defined above between absorbed/unabsorbed and variable/non-variable spectral regions. In each of these velocity bins, we also calculate the fractional change in the absorption strength,  $|\Delta A|/\langle A \rangle$ , which can have values from 0 to 2. Spectral regions that did not vary according to the criteria described above have  $\Delta A$  set to zero automatically. Note that, with  $\langle A \rangle$  and  $\Delta A$  determined in this way, each quasar can contribute more than once to these quantities in our variability analysis, depending on the range of strengths and velocities covered by its BAL troughs, because each bin showing variability is treated as a separate occurrence.

We plot the relationship between absorption strength,  $\langle A \rangle$ , and outflow velocity for all the quasars in our long-term subsample in Figure 2. A correlation between these two quantities will have implications for our results when we compare variability measures to each of these quantities individually (see §4 and §5). There is a trend for lower values of  $\langle A \rangle$  at increasing outflow velocity, which is especially apparent from  $-27,000$  to  $-8,000 \text{ km s}^{-1}$ , away from the regions of Si IV and C IV emission. The errors in the individual points are much smaller ( $\sigma_{\langle A \rangle} \leq 0.01$ ) than the dispersion of points in each bin. However, the bins at  $< -30,000 \text{ km s}^{-1}$  only contain one or two quasars, so the average  $\langle A \rangle$  in those bins can be uncertain by up to a factor of 2, given the additional uncertainty of fitting the Si IV emission line. The weaker absorption found at higher velocities in our sample is consistent with absorption in the mean BAL spectra constructed by Korista et al. (1993).

## 4 RESULTS

Table 1 indicates whether there was significant variability in the C IV BALs of each quasar in the short-term and long-term data. We found that 39% (7/18) of quasars with short-term data varied, whereas in the long-term, 65% (15/23) varied. One quasar varied only in the short-term, so com-

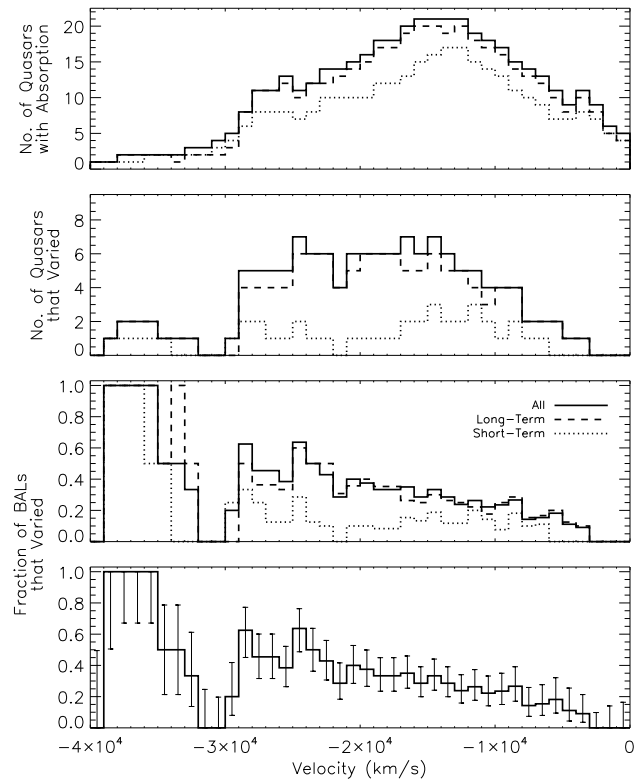


**Figure 3.** The top two panels show the number of quasars with C IV BAL absorption and the number with C IV BAL variability at each velocity. The third panel is the second panel divided by the top one, which gives the fraction of C IV BALs that varied at each velocity. The dashed, dotted, and solid curves indicate results for the long-term, short-term, and combined data set comparisons, respectively. The bottom panel displays the combined data set with  $1\sigma$  error bars.

binning both short-term and long-term data, 67% (16/24) of the quasars varied overall.

We investigated C IV BAL variability as a function of outflow velocity. Using the velocity ranges for each quasar where we have identified absorption and variability (§3.3), we count how many quasars have BAL absorption and variability in each velocity bin. In Figure 3, the top two panels show the number of quasars with C IV BAL absorption and the number with C IV BAL variability at each velocity. The third panel is the second panel divided by the top one, which gives the fraction of C IV BALs that varied at each velocity. The dashed, dotted and solid curves indicate results for the long-term, short-term and combined data set comparisons, respectively. The plot implies that BALs at higher velocities are more likely to vary than those at lower velocities.

The bottom panel in Figure 3 displays  $1\sigma$  error bars based on Wilson (1927) and Agresti & Coull (1998). These errors are based on counting statistics for the number of quasars with absorption and variability at each velocity. We perform a least-squares fit to confirm that a correlation exists between incidence of variability and velocity. The slope of the combined data is  $-1.51 \pm 0.25 \times 10^{-5}$ , in the formal unit, fraction per  $\text{km s}^{-1}$ . The slope is non-zero at a 6-sigma

significance. If we repeat the least-squares fit with only the bins with the most data (bins containing at least 8 quasars with absorption), the slope is  $-1.76 \pm 0.33 \times 10^{-5}$  fraction per  $\text{km s}^{-1}$ , which is non-zero at a 5-sigma significance. Using this restriction limits the fit to only the data from  $-29,000$  to  $-2,000 \text{ km s}^{-1}$ . We perform the least-squares fit a third time, where we restrict the fit to only the data in the range  $-27,000$  to  $-8,000 \text{ km s}^{-1}$  that completely avoids overlap with the C IV and Si IV broad emission lines. In this case, the resulting slope is  $-1.46 \pm 0.54 \times 10^{-5}$  fraction per  $\text{km s}^{-1}$ , which is non-zero at a 2.7-sigma significance. Therefore, this trend is evident even when we remove the data at the lowest and highest velocities, where additional uncertainty from the BELs can affect the results.

An important question is whether the trend seen in Figure 3 is a correlation with velocity in an absolute sense, or the cumulative result of differences between the red versus blue-side behaviors in individual absorption troughs. To address this question, we divided the velocity range of absorption for each quasar into a red and a blue half and plotted the incidence of variability separately for the red and blue portions. The result in both cases is consistent with the behavior shown in Figure 3. We do not see a higher incidence of variability in the blue portions of troughs versus the red portions. This indicates that the trend in Figure 3 is a trend in the ensemble dependent on the absolute velocity rather than the relative velocity within a given trough. Consistent with this finding is the fact that none of the BALs varied at a velocity between  $-3500 \text{ km s}^{-1}$  and  $0 \text{ km s}^{-1}$ , while the two BALs in our sample at  $<-33,000 \text{ km s}^{-1}$  both varied.

Another factor that might affect the results in Figure 3 is that BALs at higher velocities tend to be weaker (Figure 2). In Figure 4, we examine C IV BAL variability as a function of absorption strength. Using the values of  $\langle A \rangle$  calculated in §3, and a bin size of 0.05, we count how many quasars have absorption in each bin. We then count how many quasars have at least one occurrence of variability in each absorption strength bin. Each quasar is counted at most once in each bin, even if it has the same absorption strength at more than one location in the spectrum. As in Figure 3, the third panel is the second panel divided by the top one, in this case yielding the fraction of quasars with a BAL that varied in each absorption strength bin. Figure 4 indicates that quasars are more likely to exhibit BAL variability at weaker absorption strengths. As in Figure 3, we calculate errors for each absorption strength value. We again perform a least-squares fit, which gives a slope of  $-0.487 \pm 0.095$  fraction per unit absorption strength. The slope is non-zero at a 5-sigma significance. We repeat the least-squares fit with only the bins with the most data, as for Figure 3; this restricts the fit to all of the bins except the one at  $\langle A \rangle > 0.95$ . The resulting slope is  $-0.476 \pm 0.100$  fraction per unit absorption strength, which is non-zero at a 4.8-sigma significance.

Figure 4, however, does not account for multiple occurrences of the same absorption strength within an individual quasar. In §3.3, we define a method of dividing each BAL into  $\sim 1200 \text{ km s}^{-1}$  bins, and we now consider these bins as individual occurrences of absorption. In Figure 5, we plot the number of these occurrences at each absorption strength value in the top panel and then the number of these occurrences that varied in the second panel. The third panel is the

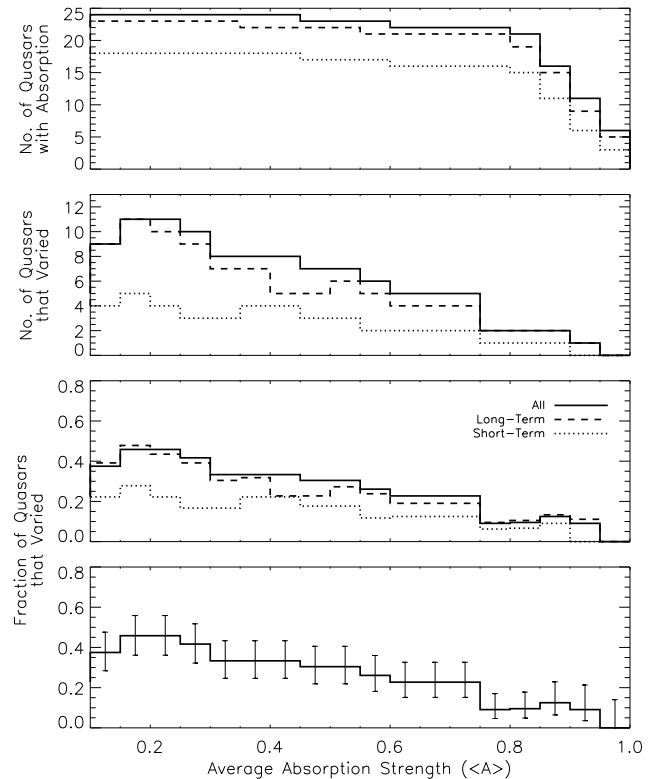


**Figure 4.** Same as Figure 3 except the quantities are plotted as a function of the normalized absorption strength, averaged between the epochs being compared.

second panel divided by the top one, showing the fraction of occurrences at each absorption strength that varied. An individual BAL may be counted more than once at each absorption strength value because we consider portions of each BAL trough in this figure. The bottom panel is the same as the third panel, except it shows just the long-term data with error bars, calculated as in Figures 3 and 4. A least-squares fit for the long-term data in Figure 5 gives a slope of  $-0.380 \pm 0.052$  fraction per unit absorption strength, which is non-zero at a 7-sigma significance. Figure 5 confirms that weaker portions of BAL troughs are more likely to vary than stronger ones.

Figures 3 to 5 compare the *incidence* of variability to properties of the BALs. Next, we use the values of  $|\Delta A|/\langle A \rangle$ , calculated in §3, to compare the *amplitude* of variability to the same BAL properties.

In Figure 6, we plot this fractional change in absorption strength as a function of the outflow velocity, using bin sizes of  $1000 \text{ km s}^{-1}$  width, as in Figure 3. In each velocity interval, the individual points represent variability in a different quasar. The average values of  $|\Delta A|/\langle A \rangle$  for just the variable (non-zero) points in each bin are shown by the open squares. The asterisks show the average if the non-varying absorption intervals are included. This plot does not indicate a statistically significant trend between fractional change in absorption strength and the outflow velocity.

In Figure 7, we plot the fractional change as a function of average normalized absorption strength, similar to Figure

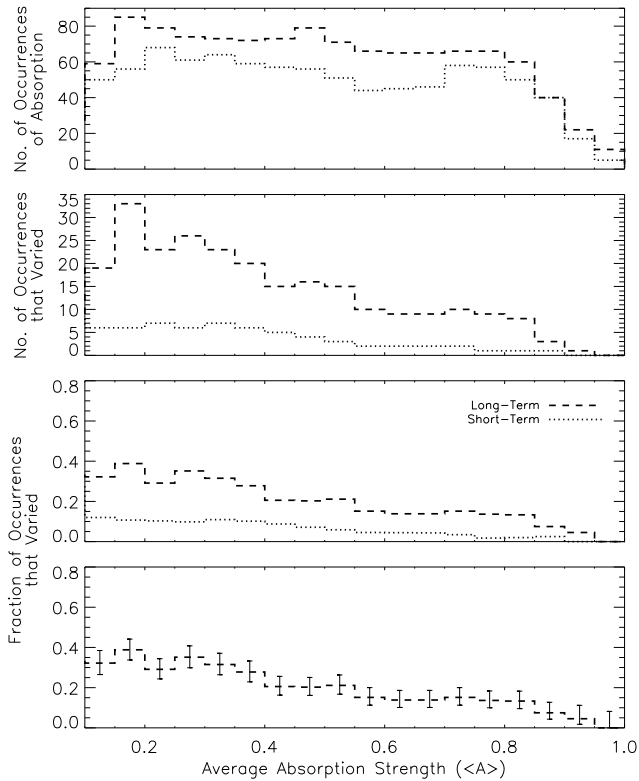


**Figure 5.** The top two panels show the total number of occurrences of absorption, and the number of those occurrences that varied, at each strength. The third panel is the second panel divided by the top one. The bottom panel displays the long-term data with  $1\sigma$  error bars.

6. In this plot, however, individual quasars will contribute multiple times to the measurements at a given absorption strength if the quasar has variability in both the red and blue sides of an absorption trough and/or in multiple troughs. The individual points represent variability at different velocities in each quasar. The average of all the variable (non-zero) points in each bin are shown by the open squares, while the asterisks show the average  $|\Delta A|/\langle A \rangle$  in each bin if non-varying absorption regions are included. This plot indicates that the fractional change in strength is greater in weaker features. However, the errors in the values of  $|\Delta A|/\langle A \rangle$  are correlated with the values of  $\langle A \rangle$ . At an  $\langle A \rangle$  of 0.15, the typical error values range from  $\sim 0.11$ - $0.33$ , whereas at  $\langle A \rangle$  of 0.60, the error values are  $\sim 0.02$ - $0.06$ . A larger error at smaller values of  $\langle A \rangle$  should cause a larger dispersion in the points in that region of Figure 7, but instead the values of  $|\Delta A|/\langle A \rangle$  converge towards the maximum possible value of  $|\Delta A|/\langle A \rangle$ . The dispersion of points due to errors in  $|\Delta A|/\langle A \rangle$  alone cannot explain the trend in this figure. Instead, this figure indicates that we see weaker absorbers, or weaker portions of BALs, appear or disappear completely, but strong features do not typically appear or disappear over the time-scales that our data cover.

Beyond looking at trends with velocity and absorption strength, it is instructive to examine the relationship between these two parameters. Figure 2 displays  $\langle A \rangle$  as a

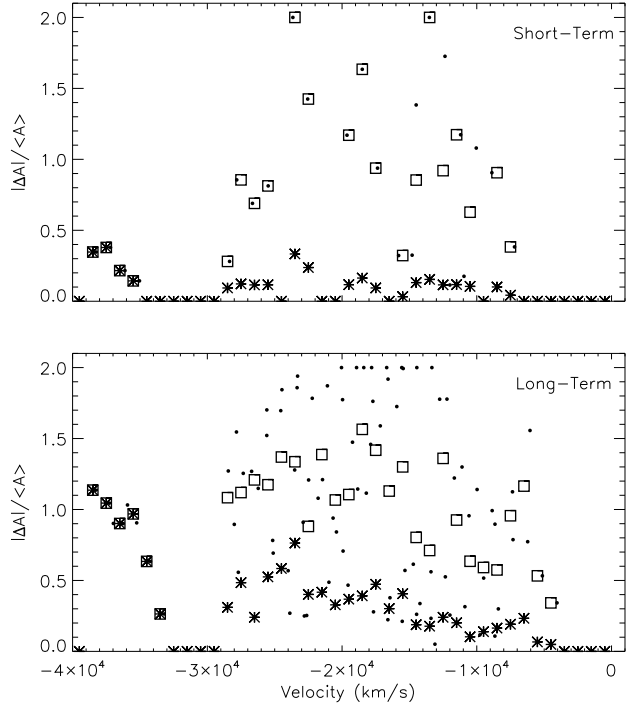


**Figure 6.** Fractional change in the depth of BAL absorption as a function of velocity. The symbols follow the same pattern as Figure 2, with individual points representing variability in a single quasar. Here, the open squares indicate the average of these variable, non-zero points in each velocity bin. The asterisks show the average  $|\Delta A|/\langle A \rangle$  in each bin if non-varying absorption intervals are included. The top panel shows the short-term results, while the bottom panel plots long-term data. We note that the maximum value of  $|\Delta A|/\langle A \rangle$  is 2 (see Figure 7), which indicates absorption appearing or disappearing completely.

function of velocity, revealing that these quantities are correlated. The lack of a clear trend in Figure 6 is surprising given that weaker systems are more variable (Figure 7) and they tend to appear more often at higher velocities (Figure 2). Evidently, the correlation of  $|\Delta A|/\langle A \rangle$  with absorption strength is stronger than the correlation with velocity. We also investigate how  $|\Delta A|$  varies with velocity and with  $\langle A \rangle$ . We do not include the plots here, but we find no trend between  $|\Delta A|$  and velocity or absorption strength.

We do not find any significant differences in the trends described above between the short-term and long-term data. The main difference is in the incidence of variability, 39% in the short-term versus 65% in the long-term data. The long-term data also show slightly larger changes in absorption strength, i.e.,  $|\Delta A|$ , compared to the short-term data. The average value of  $|\Delta A|$  is  $0.16 \pm 0.08$  in the short-term and  $0.22 \pm 0.10$  in the long-term.

We also note again that we include two quasars (0302+1705 and 0846+1540) from the Lick sample (Barlow 1993) that are not technically BALs. However, these two objects do not significantly affect the results. If we omitted them, then the fraction of quasars with variability would be 35% (6/17) in the short-term and 67% (14/21) in the long-term. In the case of 0302+1705, it does not qualify as a BALQSO because its broad absorption feature is at low ve-

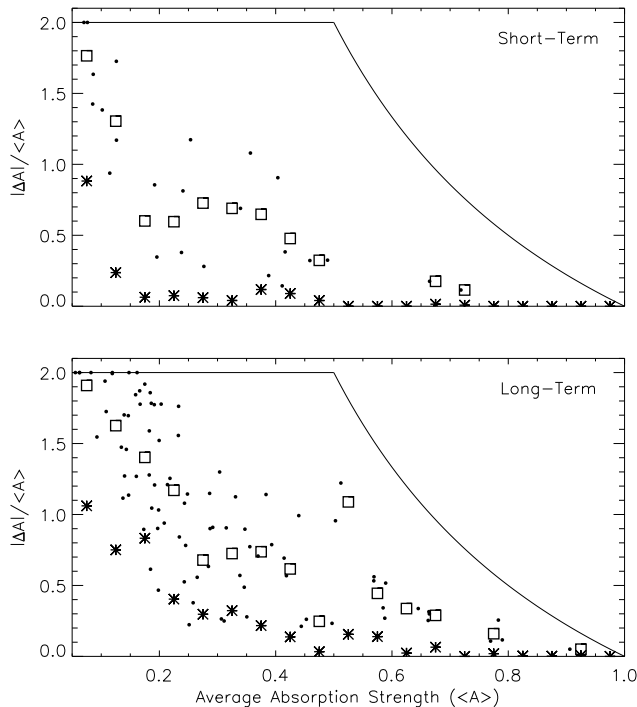


**Figure 7.** Same as Figure 6, except the fractional change is now plotted as a function of average normalized absorption strength. In this plot, individual quasars can contribute multiple times to the measurements at a given absorption strength. The solid curve represents the maximum possible value of  $|\Delta A|/\langle A \rangle$ .

locities (centered at  $\sim -2100 \text{ km s}^{-1}$ ). It also has  $\langle A \rangle$  reaching  $>0.90$ . It is a strong feature at low velocity that does not vary, fitting the trends discussed above. In 0846+1540, there is broad absorption at low velocity (centered at  $\sim -2900 \text{ km s}^{-1}$ ), with average  $\langle A \rangle$  of  $\sim 0.27$ , and at high velocity (centered at  $\sim -26,800 \text{ km s}^{-1}$ ), with average  $\langle A \rangle$  of  $\sim 0.18$ . This also fits the overall trend for higher incidence of variability at higher velocities.

## 5 SUMMARY AND DISCUSSION

We have analyzed short-term and long-term C IV  $\lambda 1549$  BAL variability in a sample of 24 quasars, and we looked for trends with the outflow velocity and absorption strength. We found that 39% (7/18) of the quasars varied in the short-term, intervals of 0.35 to 0.75 yr, whereas 65% (15/23) varied in the long-term, intervals of 3.8 to 7.7 yr. Overall, 67% (16/24) of the quasars varied. We find a trend for variability to occur more often at higher velocities (Figure 3) and in shallower absorption troughs (or shallower portions of absorption troughs; Figures 4 and 5). When looking at the fractional change in strength of the varying absorption features, there is no apparent significant correlation with velocity (Figure 6), but there is a trend for a larger fractional change in absorption strength in shallower features (Figure 7). We do include two objects with BI=0, but the variability in the broad absorption in these two quasars is consistent with the trends described above.

Gibson et al. (2008) studied C IV BAL variability on time-scales of  $\Delta t \sim 3\text{-}6$  yrs in 13 quasars with two epochs of data and found that 92% (12/13) varied. This is larger than our overall percentage of 67%. This is surprising because the selection criteria adopted by Barlow (1993) for the sample used here might be biased toward more variable sources (§2). Evidently, this bias is small or nonexistent. The difference between our result and Gibson et al. (2008) might be due to the small numbers of objects studied and/or the more conservative approach we took for identifying variable absorption.

Lundgren et al. (2007), which is a study of BAL variability on time-scales of  $<1$  yr, find an inverse correlation of fractional change in equivalent width (EW) with average EW. While EW is a different calculation than our measure of absorption strength,  $\langle A \rangle$ , encapsulating the entire BAL profile in one number instead of considering separately the different profile regions (§3.3), this result is consistent with our findings that fractional change in  $\langle A \rangle$  correlates with  $\langle A \rangle$ . Lundgren et al. (2007) also find no overall trend between fractional change in EW and outflow velocity, which is again consistent with our results. While not plotted here, we do not find a significant correlation between  $|\Delta A|$  and velocity or absorption strength, which is consistent with the analysis of Gibson et al. (2008). Gibson et al. (2008) also calculate the change in absorption strength, with values concentrated in the range 0.15-0.25. We find an average value of  $|\Delta A|$  for the long-term data of  $0.22 \pm 0.10$ .

Both Gibson et al. (2008) and Lundgren et al. (2007) comment on the lack of evidence for acceleration in the BAL features they study. We also find no evidence for acceleration in our sample. The BAL variations only involve the absorption trough growing deeper or becoming shallower. We note, however, that limits on the acceleration are difficult to quantify for BALs because, unlike narrower absorption lines, they do not usually have sharp features to provide an accurate velocity reference. BALs also exhibit profile variability, which can shift the line centroid without necessarily corresponding to a real shift in the velocity of material in the outflow.

In this work, we compare two different time intervals, and we do not find a significant difference between the short-term and long-term data in the trends described in §4. However, the incidence of variability and the typical change in strength is greater in the long-term than in the short-term. This indicates that BALs generally experience a gradual change in strength over multi-year time scales, as opposed to many rapid changes on time-scales of less than a year. This will be investigated more in a later paper where we will include all the epochs from our data set.

Variability has been investigated in other types of absorbers that are potentially related to BALs. Narayanan et al. (2004) and Wise et al. (2004) looked for variability ( $\Delta t \sim 0.3\text{-}6$  yrs) in low-velocity narrow absorption lines (NALs) and found that 25% (2/8) and 21% (4/19), respectively, of the NALs they studied varied. Rodríguez Hidalgo et al. (2010) examined variability in mini-BALs, which are absorption lines with widths larger than those of NALs and smaller than those of BALs. They observed C IV mini-BALs in 26 quasars on time-scales of  $\sim 1$  to 3 years and found variability in 57% of the sources. This number is similar to our result for BALs, however this com-

parison is complicated by a differing number of epochs and different time baselines.

Rodríguez Hidalgo et al. (2010) found no correlation between incidence of mini-BAL variability and absorption strength or outflow velocity. However, this comparison might be skewed by the fact that mini-BALs tend to be weaker than BALs. For example, none of the mini-BALs studied by Rodríguez Hidalgo et al. (2010) have depths  $A > 0.6$ , while some of the BAL features in our sample have  $A \sim 1$ . There are also differences in the velocity distributions. The mini-BAL distribution in Rodríguez Hidalgo et al. (2010) peaks at  $\sim -20,000$  km s $^{-1}$ , whereas the distribution of BAL absorption in our data peaks at  $-15,000$  to  $-12,000$  km s $^{-1}$  (Figure 3). More work is needed, e.g., with larger samples, to control for these differences in the absorption characteristics and compare BAL and mini-BAL variabilities on equal footing. Comparisons like that could provide valuable constraints on the physical similarities and relationship between BAL and mini-BAL outflows.

Two possibilities for the cause of BAL variability are the movement of gas across our line of sight and changes in ionization. We found a trend for lines at higher velocity to vary more often, which suggests movements of clouds since faster moving gas might vary more. Moreover, this is a global trend, dependent on velocity in an absolute sense, rather than relative velocity within a given trough. However, it is possible that the root cause of the variability is associated with the strength of the lines, and weaker lines happen to appear at higher velocities (see Figure 2 and Korista et al. 1993). In either case, faster moving material tends to have lower optical depths or cover less of the continuum source. Measured values of  $\langle A \rangle$  thus provide either a direct measure of optical depth, or covering fraction in the case of saturated absorption. With the current results, we cannot yet disentangle the trends in velocity and  $\langle A \rangle$  with certainty.

Evidence from BAL variability studies nonetheless supports an interpretation of varying covering factor. In addition to greater variability at higher velocities, we found changes over small portions of the BAL troughs, rather than entire BALs varying, which can be understood in terms of movements of sub-structures in the flows. Changes in the ionizing flux should globally change the ionization in the flow, and we would expect these changes to be apparent over large portions of the BAL profiles and not in just some small velocity range. Hamann et al. (2008) looked at the variation in the C IV and Si IV BALs in one quasar and found that the BALs were locked at roughly a constant Si IV/C IV strength ratio. They attribute this result to the movements of clouds that are optically thick in both lines. If the level of ionization is constant between observations or if  $\tau \gg 1$ , then the changes in absorption strength in our sample are directly indicative of changes in the covering fraction. We will examine the Si IV/C IV line ratio in our BAL data in a subsequent paper.

On the other hand, studies of NALs support the possibility of changes in ionization causing the line variability. Misawa et al. (2007) and Hamann et al. (2010) observed quasars where multiple NALs varied in concert, which suggests global changes in the ionization of the outflowing gas. If a change in ionization is causing the variability in the BAL outflows, then the optical depth ( $\tau$ ) of the BALs is changing. Features with lower optical depth are much more

sensitive to changes in ionization than those with higher optical depth. The outflowing gas is presumably photoionized by the flux from the continuum source, and changes in the continuum flux could cause a change in the ionization of the outflowing gas. However, studies to date have not found a strong correlation between continuum variability and BAL variability (Lundgren et al. 2007, Gibson et al. 2008, Barlow 1993, Barlow et al. 1992), casting doubt on ionization changes causing BAL variability.

Finally, we use the bolometric luminosities of the quasars in our sample to derive characteristic time-scales of the flows for comparison to the observed time-scales. The bolometric luminosities for the quasars in our sample range from  $\sim 2 \times 10^{46}$  to  $3 \times 10^{47}$  ergs s $^{-1}$ , and the average is  $\sim 7 \times 10^{46}$  ergs s $^{-1}$ . These values are based on the observed flux at 1450 Å (rest-frame) in absolute flux-calibrated spectra from Barlow (1993), a cosmology with  $H_o = 71$  km s $^{-1}$  Mpc,  $\Omega_M = 0.3$ ,  $\Omega_\Lambda = 0.7$ , and a standard bolometric correction factor  $L \approx 4.4\lambda L_\lambda(1450\text{\AA})$ . Based on the average value of  $L \sim 7 \times 10^{46}$  ergs s $^{-1}$ , a characteristic diameter for the continuum region at 1550 Å is  $D_{1550} \sim 0.006$  pc and for the C IV BEL region is  $D_{CIV} \sim 0.3$  pc, assuming  $L = 1/3L_{edd}$  and  $M_{BH} = 1.4 \times 10^9 M_\odot$  (Peterson et al. 2004, Bentz et al. 2007, Gaskell 2008, Hamann & Simon 2010). If the outflowing gas is located just beyond the C IV BEL region and it has a transverse speed equal to the Keplerian disk rotation speed, then the gas cloud would cross the entire continuum source in  $\sim 1$  yr. The typical time-scale in our short-term data is  $\sim 0.5$  yr and the typical change in absorption strength is at least 10%, which nominally requires the moving clouds to cross at least 10% of the continuum source. This implies transverse speeds  $> 1000$  km s $^{-1}$  and thus radial distances that are conservatively  $< 6$  pc if the transverse speeds do not exceed the Keplerian speed. A typical time-scale in the long-term data is  $\sim 6$  yr, which is enough time to cross the continuum source  $\sim 7$  times (if the gas is located just beyond the C IV BEL region). This suggests a fairly homogeneous flow for at least the cases where there is no long-term variability.

To place better constraints on the outflow properties and understand the underlying cause(s) of the line variabilities, our following papers will make more complete use of our entire data sample. We will examine the ratio of Si IV to C IV absorption to gain better insight into the cause(s) of the variability, and we will utilize more complete time-sampling instead of just looking at two specific ranges of time intervals. We have also obtained more data on BAL variability at the shortest time-scales,  $\Delta t \sim 1$  week to 1 month, in order to determine whether there is a minimum time-scale over which variability occurs. This will provide a better constraint on the location of the outflowing gas.

## ACKNOWLEDGMENTS

We thank an anonymous referee for helpful comments on the manuscript. Funding for the SDSS and SDSS-II has been provided by the Alfred P. Sloan Foundation, the Participating Institutions, the National Science Foundation, the U.S. Department of Energy, the National Aeronautics and Space Administration, the Japanese Monbukagakusho, the Max

Planck Society, and the Higher Education Funding Council for England. The SDSS Web Site is <http://www.sdss.org/>.

## REFERENCES

- Adelman-McCarthy J. K., et al., 2008, *ApJS*, 175, 297  
 Agresti A., Coull B. A., 1998, *The American Statistician*, 52, 119  
 Arnaud M., Rothenflug R., 1985, *A&AS*, 60, 425  
 Barlow, T. A. 1993, Ph.D. thesis, Univ. California, San Diego  
 Barlow T. A., Junkkarinen V. T., Burbidge E. M., Weymann R. J., Morris S. L., Korista K. T., 1992, *ApJ*, 397, 81  
 Bentz M. C., Denney K. D., Peterson B. M., Pogge R. W., 2007, *ASPC*, 373, 380  
 Di Matteo T., Springel V., Hernquist L., 2005, *Natur*, 433, 604  
 Everett J. E., 2005, *ApJ*, 631, 689  
 Gaskell C. M., 2008, *RMxAC*, 32, 1  
 Gibson R. R., Brandt W. N., Gallagher S. C., Hewett P. C., Schneider D. P., 2010, *ApJ*, 713, 220  
 Gibson R. R., Brandt W. N., Schneider D. P., Gallagher S. C., 2008, *ApJ*, 675, 985  
 Hamann F., Simon L., 2010, in preparation  
 Hamann F., Kanekar N., Prochaska J. X., Murphy M., Ellison S., 2010, in preparation  
 Hamann F., Kaplan K. F., Hidalgo P. R., Prochaska J. X., Herbert-Fort S., 2008, *MNRAS*, 391, L39  
 Hamann F., Barlow T. A., Junkkarinen V., Burbidge E. M., 1997, *ApJ*, 478, 80  
 Hamann F., Barlow T. A., Beaver E. A., Burbidge E. M., Cohen R. D., Junkkarinen V., Lyons R., 1995, *ApJ*, 443, 606  
 Korista K. T., Voit G. M., Morris S. L., Weymann R. J., 1993, *ApJS*, 88, 357  
 Lundgren B. F., Wilhite B. C., Brunner R. J., Hall P. B., Schneider D. P., York D. G., Vanden Berk D. E., Brinkmann J., 2007, *ApJ*, 656, 73  
 Misawa T., Eracleous M., Charlton J. C., Kashikawa N., 2007, *ApJ*, 660, 152  
 Moll R., et al., 2007, *A&A*, 463, 513  
 Murray N., Chiang J., Grossman S. A., Voit G. M., 1995, *ApJ*, 451, 498  
 Narayanan D., Hamann F., Barlow T., Burbidge E. M., Cohen R. D., Junkkarinen V., Lyons R., 2004, *ApJ*, 601, 715  
 Peterson B. M., et al., 2004, *ApJ*, 613, 682  
 Proga D., 2007, *ApJ*, 661, 693  
 Proga D., Kallman T. R., 2004, *ApJ*, 616, 688  
 Reichard T. A., et al., 2003, *AJ*, 126, 2594  
 Reichard T. A., et al., 2003, *AJ*, 125, 1711  
 Rodríguez Hidalgo, P., et al., 2010, in preparation  
 Shen Y., Strauss M. A., Hall P. B., Schneider D. P., York D. G., Bahcall N. A., 2008, *ApJ*, 677, 858  
 Trump J. R., et al., 2006, *ApJS*, 165, 1  
 Vanden Berk D. E., et al., 2004, *ApJ*, 601, 692  
 Vanden Berk D. E., et al., 2001, *AJ*, 122, 549  
 Weymann R. J., Morris S. L., Foltz C. B., Hewett P. C., 1991, *ApJ*, 373, 23  
 Weymann R. J., Williams R. E., Peterson B. M., Turnshek D. A., 1979, *ApJ*, 234, 33  
 Wilhite B. C., Vanden Berk D. E., Kron R. G., Schneider D. P., Pereyra N., Brunner R. J., Richards G. T., Brinkmann J. V., 2005, *ApJ*, 633, 638  
 Wilson E. B., 1927, *Journal of the American Statistical Association*, 22, 209  
 Wise J. H., Eracleous M., Charlton J. C., Ganguly R., 2004, *ApJ*, 613, 129